PLOS | ONE

RESEARCH ARTICLE

Dynamic Responses of Selective Brain White Matter Fiber Tracts to Binge Alcohol and Recovery in the Rat

Adolf Pfefferbaum[1,2], Natalie M. Zahr[1,2]*, Dirk Mayer[1,3], Torsten Rohlfing[1], Edith V. Sullivan[2]

1 Neuroscience Program, SRI International, Menlo Park, CA, United States of America, **2** Department of Psychiatry and Behavioral Sciences, Stanford University School of Medicine, Stanford, CA, United States of America, **3** Department of Diagnostic Radiology, University of Maryland School of Medicine, Baltimore, MD, United States of America

* nzahr@stanford.edu

Citation: Pfefferbaum A, Zahr NM, Mayer D, Rohlfing T, Sullivan EV (2015) Dynamic Responses of Selective Brain White Matter Fiber Tracts to Binge Alcohol and Recovery in the Rat. PLoS ONE 10(4): e0124885. doi:10.1371/journal.pone.0124885

Academic Editor: Alessandro Gozzi, Italian Institute of Technology, ITALY

Received: September 24, 2014

Accepted: March 18, 2015

Published: April 20, 2015

Data Availability Statement: Data are from the labs of Drs. Pfefferbaum (dolf@synapse.sri.com) and Sullivan (edie@stanford.edu). Nifti files of FA data for each rat at each time point are available at figshare (http://figshare.com/) at the following URL: http://figshare.com/articles/Dynamic_Responses_of_Selective_Brain_White_Matter_Fiber_Tracts_to_Binge_Alcohol_and_Recovery_in_the_Rat/1330402.

Funding: National Institute on Alcohol Abuse and Alcoholism: AA005965, AA012388, AA017168, AA013521-Integrative Neuroscience Initiative on Neuroscience (INIA). SRI International is a nonprofit center (http://www.sri.com/about). The funders had no

Abstract

To determine the dynamics of white matter vulnerability to excessive alcohol consumption, diffusion tensor imaging (DTI) was used in an animal model of alcohol exposure. Quantitative, *in vivo* fiber tracking results are presented from rats with DTI conducted at 3 time points: baseline; after 4 days of intragastric alcohol to blood alcohol levels of ~250mg/dL; and after one week of recovery. Binge alcohol followed by a week of sobriety resulted in rapidly reversible decreases in fractional anisotropy (FA), a measure of the coherence of fiber tracts, in callosal genu and fimbria-fornix but not splenium; and increases in mean diffusivity (MD), an index of freely diffusing water in tissue, selective to the fimbria-fornix. These effects were confirmed with tract-based spatial statistics (TBSS). The directionality of changes in DTI metrics reproduce those observed in human alcoholism. That a single exposure to binge alcohol can cause substantial transient changes detectable in DTI metrics demonstrates the potential for rapid neuroplasticity.

Introduction

Postmortem studies of human cases of alcohol use disorders (AUD) suggest that brain volume reductions are largely accounted for by shrinkage of white matter [1–3]; for example, the corpus callosum is significantly thinned [3–5]. In vivo, disruption of white matter integrity in chronic alcoholism can be detected with diffusion tensor imaging (DTI) [6–10] and can be more sensitive than measures of macrostructure (i.e., white matter volume) for detecting the throes of alcoholism [11,12].

Metrics of DTI provide indices of different features of fiber condition: fractional anisotropy (FA) indexes the degree of coherence of fiber tracts and ranges between 0 (lowest) to 1 (perfect linearity), and mean diffusivity (MD) is indicative of unrestricted water movement and reflects some aspects of tissue architecture [13–18]. Two derivative measures of mean diffusivity provide indices of selective features of white matter tracts: longitudinal diffusivity (also called

role in study design, data collection and analysis, decision to publish, or preparation of the manuscript.

Competing Interests: The authors have declared that no competing interests exist.

axial, λ_L) is thought to reflect axonal integrity, whereas transverse diffusivity (also called radial, λ_T) is thought to reflect myelin integrity [19–21]. A common finding in adult human alcoholism is evidence for greater degradation (lower FA and higher MD with λT particularly affected)[22] of anterior (e.g., genu, anterior cingulate bundle, and frontal forceps) than posterior (e.g., splenium) white matter fiber tracts [7,8,11,23–27]. Mechanisms of alcoholic white matter injury, however, remain unknown.

Animal studies permit the interrogation of factors underlying white matter sensitivity to alcohol exposure. Animal models of components of human AUD enable control over relevant variables, such as amount, length, and pattern of alcohol exposure [28,29]. A variety of methods are available for exposing animals to alcohol and include vapor inhalation, intragastric infusion, and voluntary drinking. The 4-day binge protocol has been used extensively to model alcoholism in rodents because sustained blood alcohol level (BAL) elevations by intragastric alcohol administration have been shown as adequate for rapid induction of physical dependence in the rat [e.g., 30,31].

Although other studies have examined white matter tracts in rodents [32,33], to our knowledge, only one study measured DTI metrics in response to alcohol exposure in the rat: a single intragastric dose of alcohol resulted in mild decreases in the apparent diffusion coefficient (ADC, a DTI metric similar to MD) and no effects on FA [34]. This decrease in ADC is distinct from typical findings in humans with chronic alcoholism [8,24–27] and may be due to a species (rat vs. human) or alcohol exposure (acute vs. chronic) effects. To expand on this previous DTI finding in a more typically implemented animal model of alcohol exposure, the present study performed *in vivo*, quantitative fiber tracking on DTI data acquired in rats exposed to short-term binge alcohol *via* intragastric gavage [35]. We tested two principal hypotheses: 1) *in vivo* DTI in the rat would detect selective changes to white matter in response to binge alcohol exposure with greater abnormalities (lower FA and higher MD) in anterior than posterior fiber systems; and 2) as observed for ventricular volume and metabolite changes [35], disruption of fiber tracts would be transient, showing normalization with one week of recovery from alcohol. To minimize bias in selecting a limited number of white matter tracts to quantify, we also analyzed data using tract-based spatial statistics (TBSS), which determines DTI metrics in the whole white-matter skeleton of the brain.

Materials and Methods

Ethics Statement

The Institutional Animal Care and Use Committees at SRI International (protocol #01019) and Stanford University (protocol #8800) approved all procedures.

Alcohol Treatment and Schedule

The study group initially included 22 wild-type, male Wistar rats (Charles River Laboratories) weighing 334.83±3.7g at baseline, singly housed with free access to food and water, with lights on for 12 hours starting at 8:00. DTI was conducted at 3 sequential magnetic resonance (MR) scanning sessions: DTI 1—pre-treatment baseline; DTI 2—following 4 days of intragastric gavage of alcohol or dextrose (control); and DTI 3—following one week of recovery, that is, without alcohol (Fig 1). This same group of rats underwent examination with structural MR imaging and MR spectroscopy at the same MR scanning sessions [35].

After baseline scanning, 11 rats were assigned to the alcohol group and received an initial "loading" dose of 5g/kg 25% alcohol w/v *via* oral gavage, then a maximum of 3g/kg every 8 hours for 4 days. On each of the 4 days, animals were weighed and tail vein blood samples were collected to determine BALs in plasma assayed for alcohol content based on direct reaction

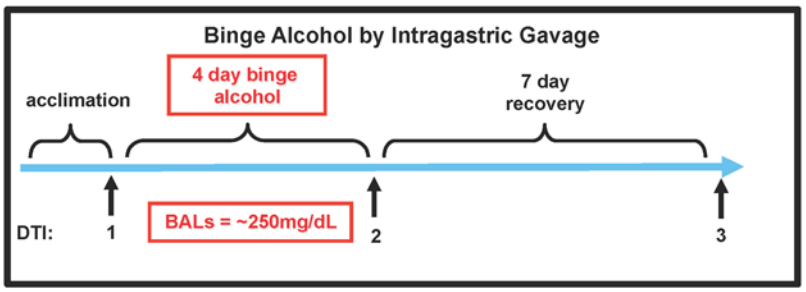

Fig 1. Schedule of alcohol exposure.

doi:10.1371/journal.pone.0124885.g001

with the enzyme alcohol oxidase (Analox Instruments Ltd., UK). Target BALs were 250mg/dL because alcohol dependent individuals show normal motor function at fairly high alcohol levels (200–400mg/dL) [36,37]. Alcohol was administered according to body weight, BALs, and behavioral signs of intoxication. Dosing was adjusted for each animal so that less than 3g/kg was administered if the animal's behavior or BALs indicated that it was still too intoxicated from the previous dose to receive the full 3g/kg dose. Specifically, doses were determined individually for each animal according to the published schedule described by correlations between BALs and severity of intoxication [38]: the greater the severity of intoxication, the smaller the dose of alcohol administered [39]. Daily doses averaged 7.21±.32g/kg/animal (cumulative dose across 4 days = 28.85±1.26g/kg/animal) at a daily volume averaging 8.87±.46mL/animal. Control animals received volumes of 5% dextrose equivalent to 3g/kg alcohol (daily volume averaging 11.86±.43mL/animal) at comparable times to the experimental animals, i.e., ~7:00, 15:00, and 23:00. The alcohol dose was titrated based on BALs and behavioral intoxication states, whereas dextrose was given at a constant volume based on 3g/kg alcohol per day; thus the control group received a greater fluid load than the alcohol group ($t(19) = 4.75$, $p = .0001$). These methods resulted in average BALs of ~250mg/dL in the alcohol-treated rats. Two alcohol and one control rat received baseline and binge scans but died before the recovery scans.

MRI Acquisition

Following our established protocol [35,40,41], each animal was held in an MR-invisible structure, which provided support for the radiofrequency (RF) coil and a nose cone for the delivery of isoflurane anesthesia (1–2%) and oxygen (~1.5 l/min). Rectal temperature and oxygen saturation from the hind limb were monitored throughout the duration of the 2-hour MR acquisition. A pad of warmed saline placed under the animal provided heating.

The experiments were conducted on a clinical 3T GE Signa human MR scanner equipped with a high-strength insert gradient coil (peak strength = 600 mT/m; peak slew rate = 3200 T/m/s) [41–43]. As previously described [44], the gradient system was operated at a maximum amplitude of 500 mT/m with a slew rate of 1800 mT/m/ms to minimize vibration and acoustic problems. A custom-made rat brain quadrature head coil (∅ = 44 mm) was used for both RF excitation and signal reception.

A gradient recalled echo (GRE) localizer scan (echo time (TE)/repetition time (TR) = 2.1/24.6 ms, flip angle = 30°, field of view (FOV) = 80×80 mm^2, 256×128 matrix, three 5-mm slices per plane, scan time = 47 s) was used to position the animals in the scanner and for graphical prescription of the fast spin-echo (FSE). Dual-echo, FSE images were acquired in the axial plane (coronal to the magnet system bore; TE1/TE2/TR = 11.3/56.7/7000 ms, FOV = 60×60 mm^2, 256x256 matrix, echo train length of 8, or 26 contiguous slices, 0.7mm thick). The FSE data were used for the prescription of the DTI acquisition sequence.

The RF and gradient scheme of the implemented DTI echo-planar pulse sequence (FOV = 32×32 mm^2, TE/TR = 32.8/2000 ms) was previously published [44]. Multi-slice data were acquired in axial orientation (magnet coronal) at in-plane resolution of 0.5 mm and through-plane resolution 0.7 mm, with and without diffusion weighting. A partial k-space acquisition scheme (n_{read} = 64, n_{phase} = 48) was applied to reduce TE. Frequency encoding direction was left to right. Data were acquired with a readout bandwidth of ±200 kHz (G_{read} = 147 mT/m) and an echo spacing of 0.544 ms for a total readout duration of 26.1 ms. Symmetric diffusion-weighting gradients were applied with a b-value = 1464 s/mm^2 in 6 noncollinear directions (+x+y, +y+z, +x+z, -x+y, -y+z, +x-z); the same 6 directions with opposite polarity were acquired to compensate for the cross-terms caused by both imaging and crusher gradients [45]. Six directions are the minimum needed to define the diffusion tensor, and we chose to enhance single-shot signal-to-noise ratios with multiple averages of the same direction rather than using more directions with fewer averages. Crusher gradients to dephase transverse magnetization resulting from imperfect refocusing pulses were applied in all 3 directions immediately before and after the 180° pulse. Frequency-selective lipid suppression and outer-volume suppression modules preceded the imaging sequence. Saturation bands were placed around the FOV. Six averages per acquisition were collected with the positive and negative polarity gradient scheme and repeated 12 times for a total DTI acquisition time of 45 min.

DTI Analysis

DTI quantification was preceded by eddy-current correction on a slice-by-slice basis using within-slice registration, which takes advantage of the symmetry of the opposing polarity acquisition [46]. The reversing diffusion gradient polarity scheme also eliminates the need to account for the cross terms between imaging and diffusion gradients by averaging the opposite polarity data [45], reducing the data to six non-collinear diffusion-weighted images per slice. Using the field maps, B0-field inhomogeneity-induced geometric distortion in the eddy-current corrected images was attenuated with PRELUDE (Phase Region Expanding Labeller for Unwrapping Discrete Estimates)[47] and FUGUE (FMRIB's Utility for Geometrically Unwarping EPIs; http://www.fmrib.ox.ac.uk/fsl/fugue/), although this procedure had minimal effect on the data. The basis images were interpolated to .125 mm isotropic resolution with a windowed sinc in-plane and linear through-plane function and smoothed with a 3×3×3 boxcar average. DTI metrics (FA, MD, longitudinal diffusivity [λ_L], and transverse diffusivity [λ_T]) were computed with standard tensor fitting methods [17].

Fiber Tracking

The genu, splenium, and bilateral fimbria-fornix tracts of the hippocampus were identified as point targets in the FSE image of a laboratory standard animal, which was selected based on image quality (e.g., low image noise, no visible artifacts) and animal positioning (e.g., centered within the available FOV with no cropping). The baseline late-echo FSE anatomical images were registered nonrigidly [48](http://nitrc.org/projects/cmtk) to the standard animal image. We used the Normalized Cross-Correlation similarity measure to drive the registration, which used a three-level B-spline transformation [49] with a final control point spacing of approximately 0.7 mm (the exact control point spacing is a function of the initial control point spacing, here 2.5 mm, the number of grid refinement steps, here 2, and the image field-of-view).

For each follow-up session, each animal's image FSE was also registered nonrigidly to the same animal's baseline FSE image. The target point locations were then mapped from the standard animal space into native space for each animal and session using the aforementioned registration to the standard animal space (for the baseline session) or the concatenation of the

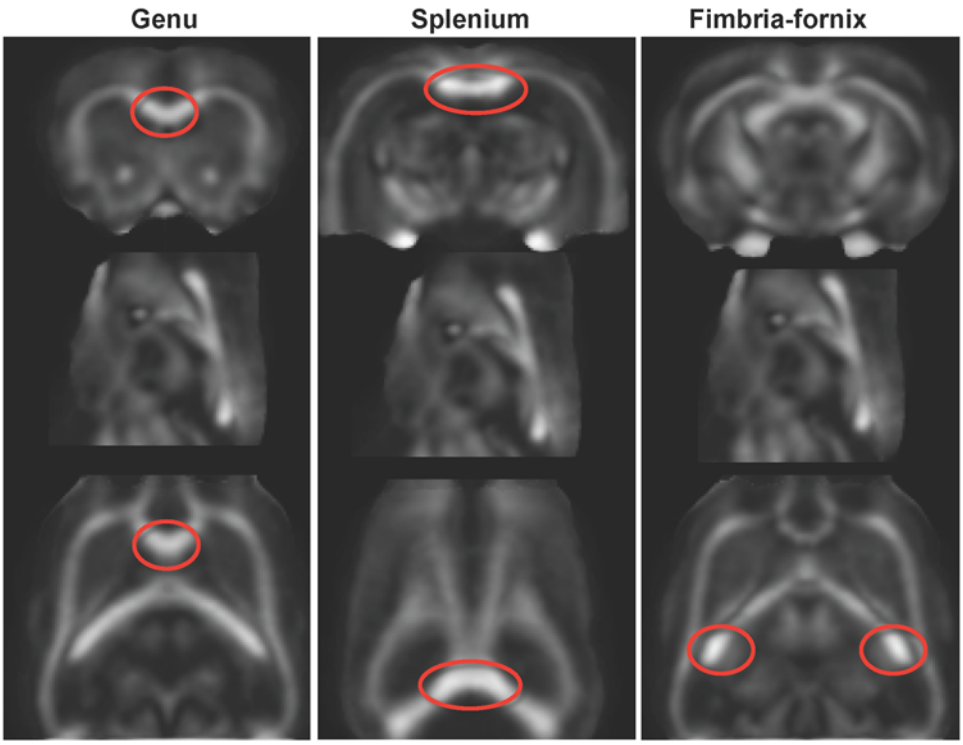

Fig 2. FA maps with circles indicating regions of the genu (right) and splenium (middle) of the corpus callosum and fimbria-fornix (left) used for fiber tract quantification of FA and MD.

doi:10.1371/journal.pone.0124885.g002

standard-to-baseline with the baseline-to-follow-up registration. For longitudinal studies we have found that, while there is likely a small increase in absolute registration error due to concatenation, a sequential approach significantly reduces the inconsistency of quantification across time points [50].

To improve the precision of target locations, an automated 5-point, 3-dimensional local maximum search within the FA image ensured location of the target within the center of the given fiber track. The identified point was then expanded to a target, which was a 7 x 7 plane, 3-voxels thick, perpendicular to fiber orientation. Thresholds used included an FA value limit of .17 and an angle maximum of 37°. Tracking sources were automatically defined as planes parallel to the genu and splenium targets and anterior/posterior to the fimbria-fornix. Quantitative fiber tracking routines and parameters, developed by Mori and Xu [51,52] and distributed by G. Gerig [53] (www.ia.unc.edu/dev/download/fibertracking), were used and produced pictorial fiber bundle representations. Quantification of the mean FA and MD of the fibers were similar to those we have previously used *in vivo* in the human brain [7,54] and rat brain [44]. Mean FA and MD were calculated for fibers of the genu and splenium of the corpus callosum, and left and right fimbria-fornix tracts (Fig 2).

Tract Based Spatial Statistics (TBSS)

For TBSS analysis, the structural registrations to the aforementioned laboratory standard were used to reformat each animal's FA image into common space. As described above for tracking target transformation, we used concatenated standard-to-baseline and baseline-to-follow-up registrations to reformat the FA image from the follow-up images of all animals, again to reduce the longitudinal inconsistency the registrations. Initial mean FA image and FA skeleton

were constructed, with the skeleton extraction threshold set at FA = 0.20. Contrasts were performed for alcohol vs. control (dextrose) at DTI 2. Statistical testing was performed using TFCE (Threshold-Free Cluster Enhancement) [55] with 1000 permutations. The resultant clusters were examined for voxels meeting $p \leq .05$ fully corrected for multiple comparisons across space.

Statistical Analysis

Principal differences between alcohol-exposed and control groups were tested with repeated-measures analysis of variance (ANOVA) across imaging sessions, where group (i.e., alcohol or control)-by-session (i.e., DTI 1, DTI 2, DTI 3) interactions would provide support for potential effects of alcohol treatment. ANOVAs were conducted using lme in R (http://www.r-project.org/) for data from rats that completed at least the first two DTI sessions (control = 10, alcohol = 9; two alcohol and one control rat had only DTI 1 and DTI 2 data available for analysis). The lme allowed the ANOVA to be calculated using all data and accounting for empty cells (i.e., missed sessions). Follow-up t-tests were employed where needed with appropriate adjustment for multiple comparisons. Relations between variables were tested with Pearson correlations and verified with nonparametric Spearman rank-order correlations because of the small samples.

Results

Repeated-measures ANOVAs for FA of each fiber track yielded group-by-session interactions in the genu ($F(2,55) = 4.95$, $p = .010$) but not the splenium ($F(2,55) = .88$, $p = .42$) (Fig 3). Interactions were also significant for both the left ($F(2,55) = 7.91$, $p = .0009$) and right ($F(2,55) = 6.09$, $p = .004$) fimbria-fornix tract (Fig 4). In all cases, paired t-tests indicated that the interaction was attributable to a significant drop in FA from the first to the second DTI session followed by a return in FA, observed in the alcohol but not the control group. For MD, the alcohol effect, identified as group-by-session interactions, was limited to the fimbria-fornix: left ($F(2,55) = 8.71$, $p = .0005$) and right ($F(2,55) = 11.40$, $p = .00007$). In complement to FA, the interaction indicated a rise in MD followed by a return to baseline in the alcohol-treated group only. One control animal had an exceptionally high MD at DTI 2, but the results were the same with or without its data in the analysis. ANOVAs based on data from animals that completed two or more DTI sessions yielded the same results as the ANOVAs based on rats with complete sessions.

Two-group-by-three session interactions were also significant for λ_L ($F(2,55) = 4.44$, $p = .02$) but not λ_T ($F(2,55) = 1.88$, $p = .16$) in genu (Fig 5). Here the pattern of changes were similar to FA, that is, attributable to a drop in λ_L from DTI 1 to DTI 2, followed by a return of λ_L to baseline levels at DTI 3, in the alcohol but not control group. Significant group-by-session interactions were noted for both λ_L (left: $F(2,55) = 3.42$, $p = .04$; right: ($F(2,55) = 5.45$, $p = .007$) and λ_T (left: $F(2,55) = 10.94$, $p = .0001$; right: ($F(2,55) = 12.5$, $p = .00003$) in fimbria-fornix, but followed the MD pattern, that is, both were elevated at DTI 2 but returned to baseline at DTI 3 in the alcohol-treated group only (Fig 6). The same patterns were present in the groups including animals that only completed the first two scanning sessions.

TBSS Results

Fig 7a shows axial and coronal TBSS maps demonstrating white matter skeleton voxels (in orange) with lower FA in alcohol-exposed than in dextrose-treated animals at DTI 2. At DTI 3, the alcohol-treated rats had ~900 voxels with lower FA than the dextrose-treated control rats at $p < .02$; ~850 voxels differed at $p < .001$. Most voxels with lower FA at DTI 2 were in the genu and lateral extent of the corpus callosum, the fimbria-fornix and frontal forceps (Fig 7b, in

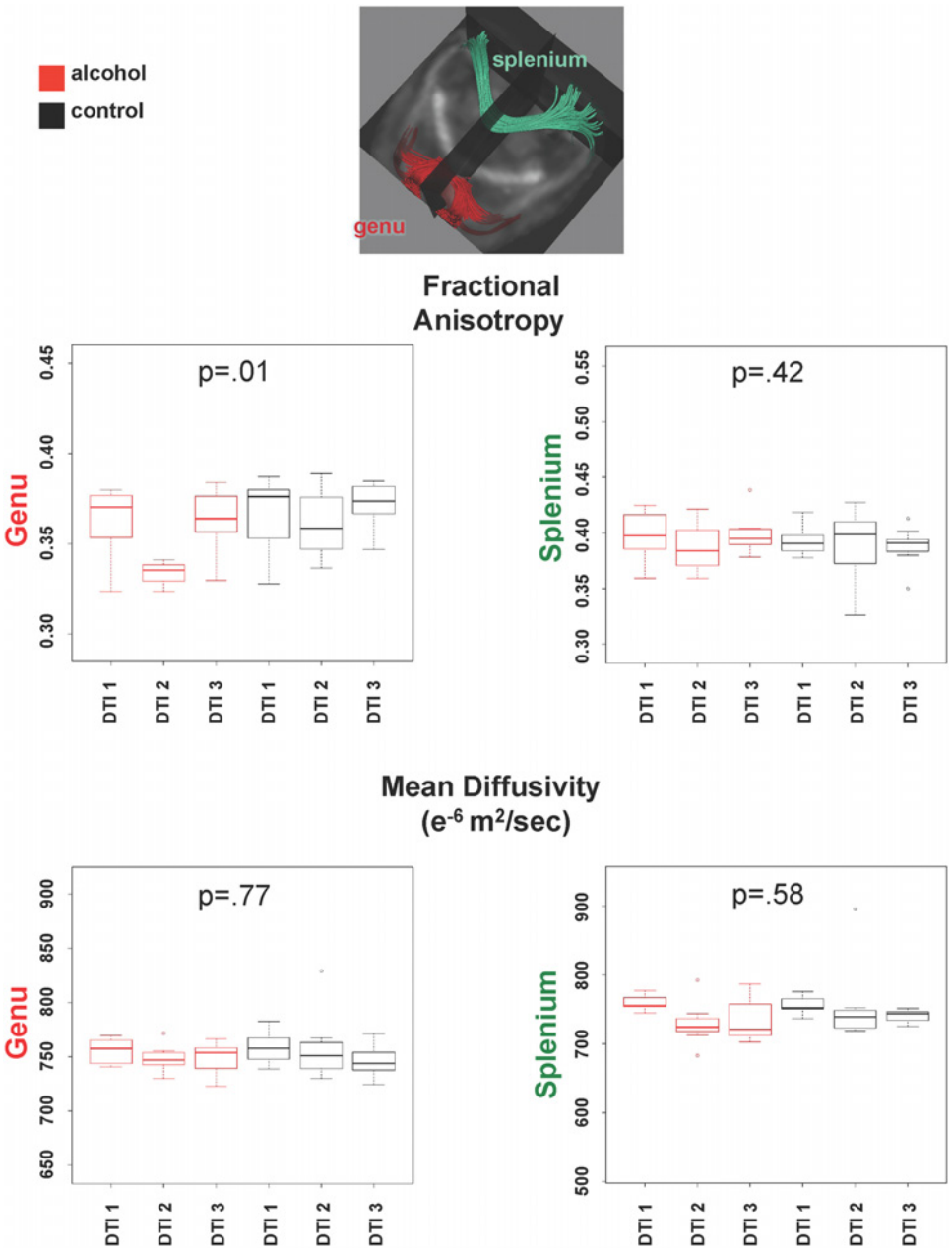

Fig 3. Inset shows fiber tracts of the genu (red) and splenium (green). Graphs show quantified results of FA (top) and MD (bottom) in corpus callosum genu and splenium. Dots here an in consequent graphs represent outliers.

doi:10.1371/journal.pone.0124885.g003

orange). No voxel met $p<.05$ criterion for opposite contrast of lower FA in dextrose- than alcohol- exposed animals. A comparison between alcohol- and dextrose- treated animals at DTI 3 showed minimal FA differences (at $p<.05$ family-wise error corrected, Fig 7b, in blue).

DTI findings and alcohol levels

To examine the effect of the full extent of the alcohol binge treatment on the DTI metrics, we tested the relation between DTI metrics and average BALs attained during the 4-day binge.

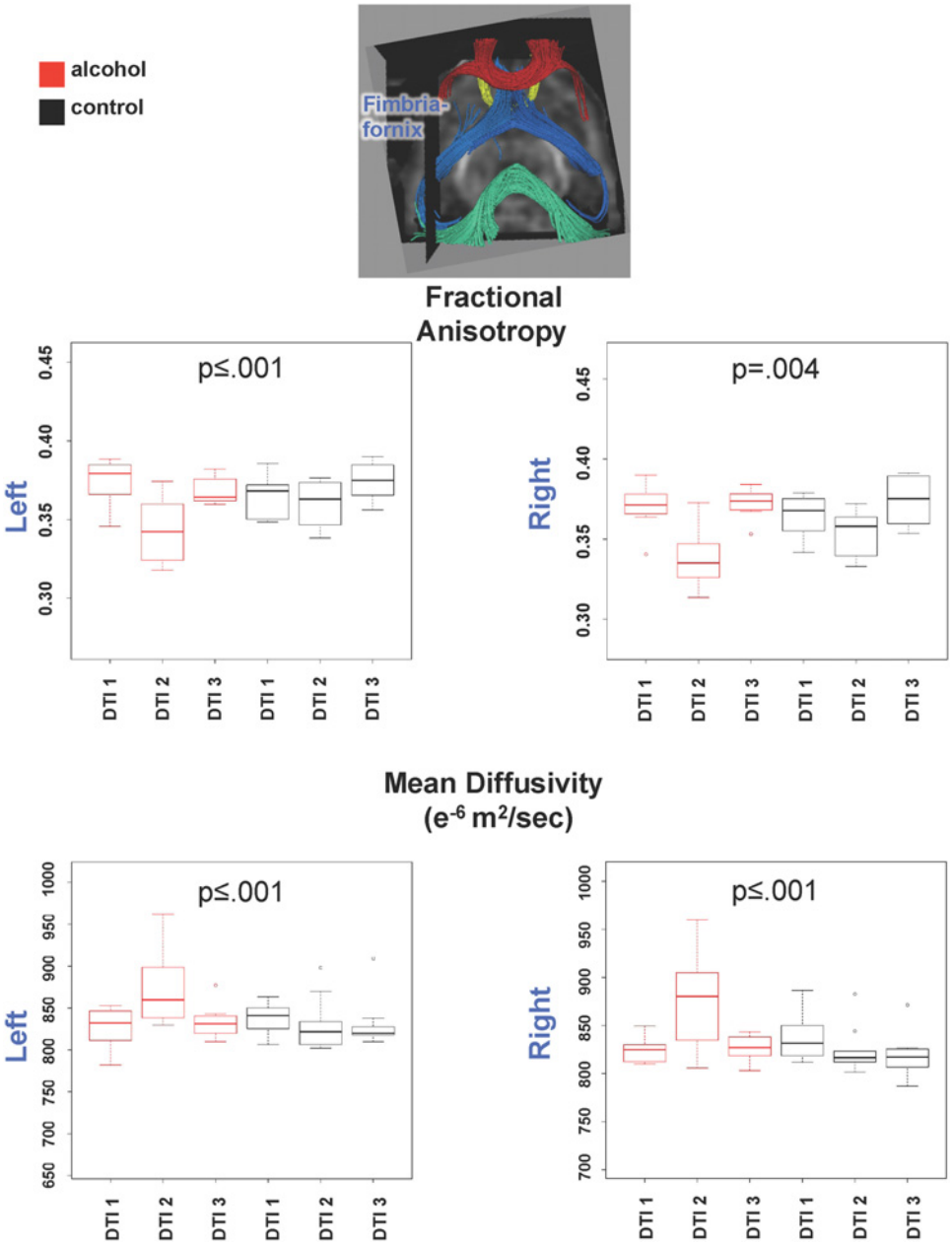

Fig 4. Inset shows fiber tracts of the fimbria-fornix (blue). Graphs show quantified results of FA (top) and MD (bottom) in left and right fimbria fornix.

doi:10.1371/journal.pone.0124885.g004

None of the correlations for genu or splenium FA or MD was significant. By contrast, for the fimbria-fornix, higher average BALs obtained during binge sessions correlated modestly with lower FA at DTI 2 (bilateral: Rho = -.65, p = .04; right: Rho = -.68, p = .03, left: Rho = -.58, p = .08) (Fig 8).

Discussion

Binge alcohol exposure, resulting in BALs of ~250mg/dL, produced reversible changes in indices of white matter microstructural integrity of selective fiber tracts: the genu and fimbria-fornix of

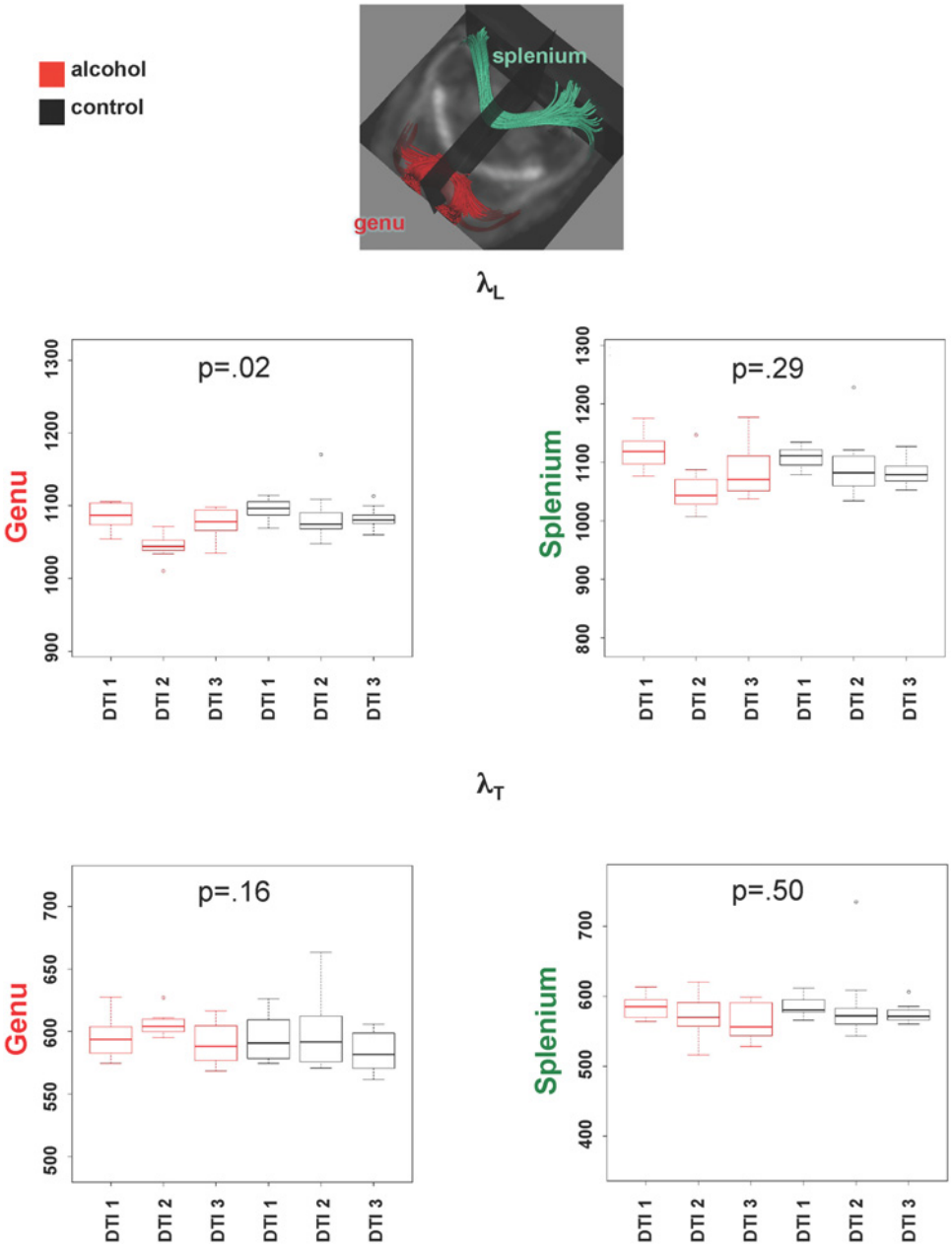

Fig 5. Graphs show quantified results of λ_L (top) and λ_T (bottom) in corpus callosum genu and splenium.

doi:10.1371/journal.pone.0124885.g005

the hippocampus were affected (FA was substantially lower in genu and fimbria-fornix systems, and MD was higher in fimbria-fornix), while the splenium was spared. The directionality of FA and MD changes comports with findings in chronically drinking alcoholic humans showing a focal vulnerability of anterior white matter fiber systems, quantified as lower FA and higher MD in cross-sectional study [7,8,11,23–27] and longitudinal follow-up [12,56]. We also report changes in λ_L and λ_T: in the genu, λ_L was lower following binge alcohol treatment and returned to baseline levels with recovery; in the fimbria-fornix, λ_L, and λ_T were both higher with binge treatment and returned to baseline with recovery. Trends suggested that the lower FA was

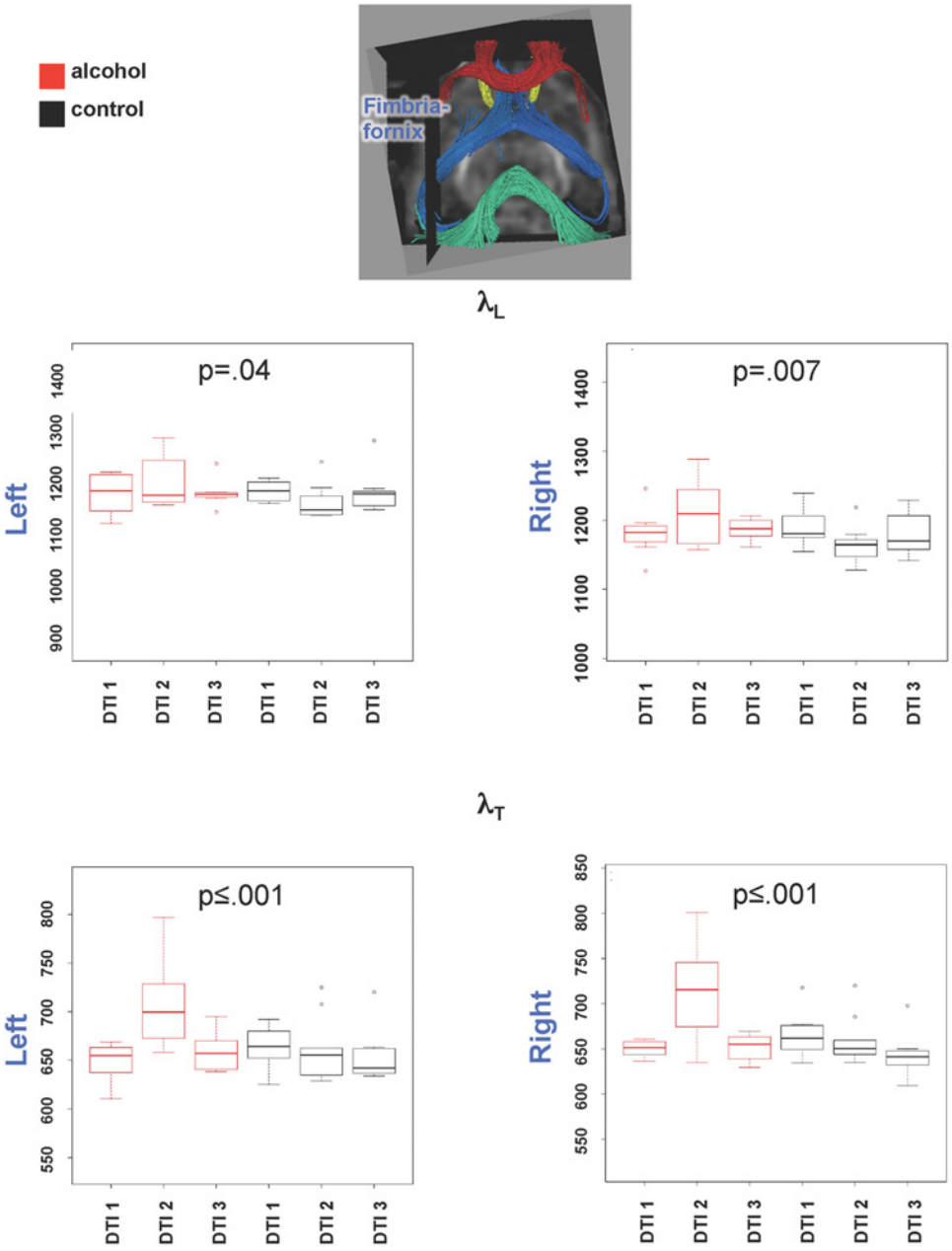

Fig 6. Graphs show quantified results of λ_L (top) and λ_T (bottom) in left and right fimbria fornix.

doi:10.1371/journal.pone.0124885.g006

related to the cumulative effects of the binge treatments, i.e., total average BALs achieved during the 4 days of binge alcohol exposure. To our knowledge, this is the first demonstration of a relationship between BALs and brain DTI metrics.

A potential limitation of the current study is that the DTI changes observed as a consequence of binge alcohol treatment are the result of partial volume effects of quantification of fiber pathways near the ventricles, which our previous study noted were enlarged [35]. Two results mitigate against that conclusion. Firstly, if partial volume effects were responsible for the quantified DTI changes in response to binge alcohol, both the genu and the splenium, structures similarly adjacent to the ventricles, should have shown altered DTI metrics. Secondly, the

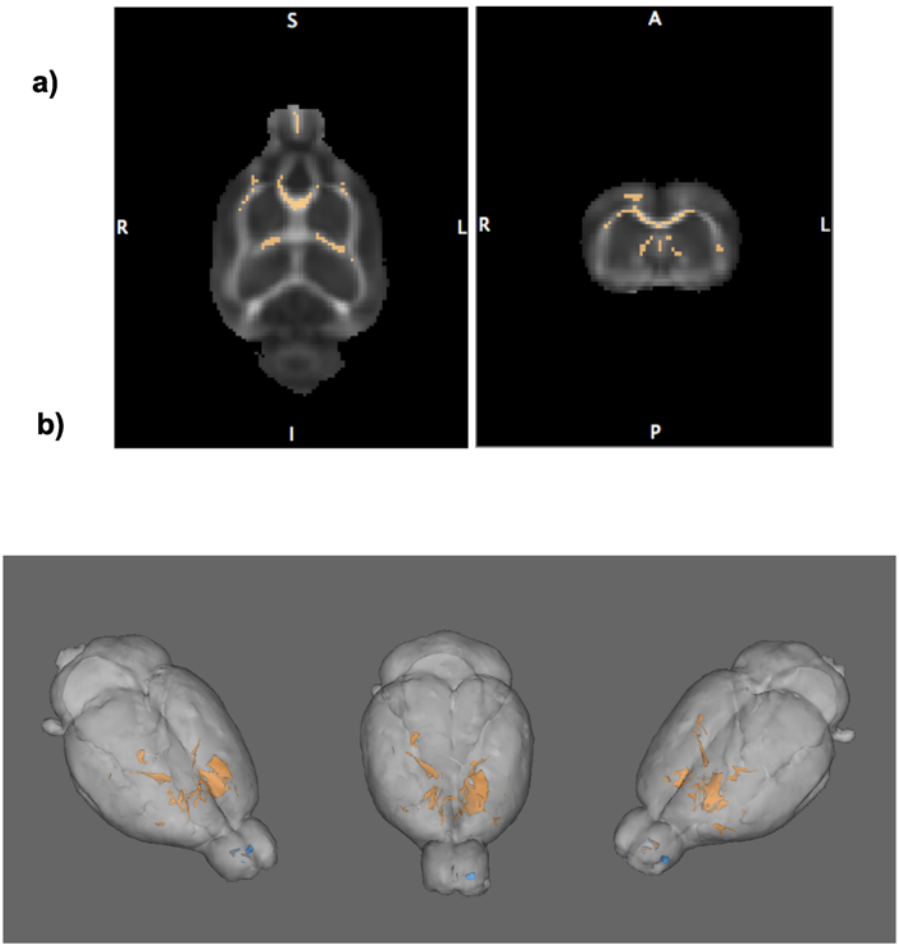

Fig 7. a) Axial and coronal FSL presentations of a rat white matter skeleton indicating voxels with lower FA in alcohol-exposed than dextrose-treated animals after acute binge treatment (i.e., DTI 2). b) TBSS results in 3D at DTI 2 (orange) show where FA was lower in the alcohol than dextrose treated animals at p<.02. In blue are indicated the voxels showing FA differences between alcohol-exposed than dextrose-treated animals at DTI 3.

doi:10.1371/journal.pone.0124885.g007

fiber tracking results were corroborated by TBSS, which is less prone to partial voluming effects [57] and showed that the genu, but not the splenium responded to binge alcohol exposure. Another potential limitation is that forced alcohol exposure is a simple method to evaluate questions regarding the effects of high alcohol levels on neuropathology but does not model free-choice drinking. High alcohol drinking in AUD is mediated by complex neurobiological, environmental, and behavioral interactions, and animal models of free-choice drinking have greater validity than forced exposure [58]. However, an alcohol deprivation effect model used in alcohol preferring (P rat) [59,60] and in high alcohol drinking (HAD rat) lines [61,62] demonstrates free-choice drinking to BALs of only 80mg% and a drinking in the dark, multiple scheduled access procedure also using selectively bred rats (P and HAD rats) similarly achieves BALs approaching only 80mg% [63,64]; thus, free choice drinking in rodent models fails to approach levels frequently achieved by heavy drinkers (>200mg%) [65–70]. Finally, ideally, isotropic acquisition is the best approach. However, signal-to-noise constraints make this impractical so the standard compromise is to have higher resolution in-plane than through- plane and to recognize that the 3D reformatting has this limitation

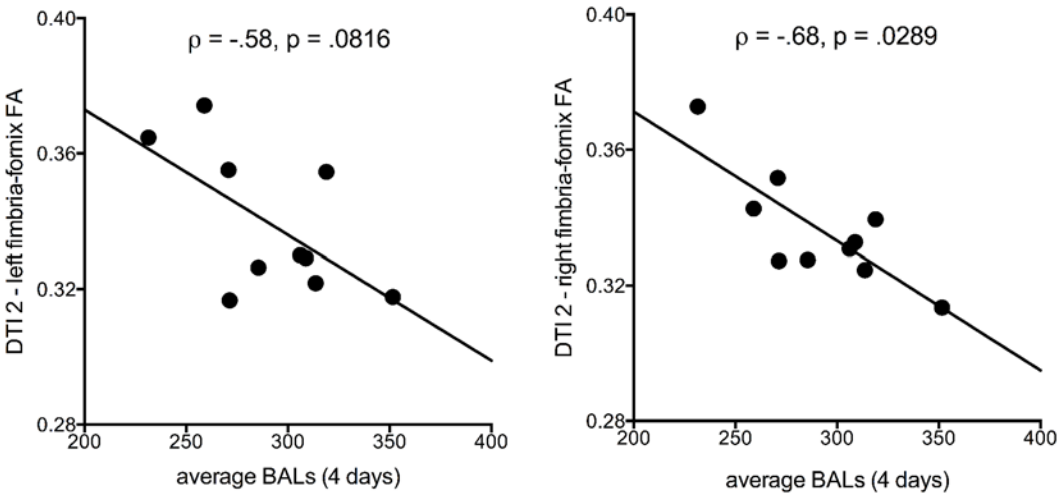

Fig 8. Correlations between left and right fimbria-fornix FA and average BALs across the 4 days of binge alcohol treatment. Bilateral results were also significant (Rho = -.65, p = .0425).

doi:10.1371/journal.pone.0124885.g008

Recent evidence from both human and animal studies indicates the potential for rapid changes in DTI-derived measures [71–73]. Here, the genu in response to binge alcohol exposure showed a pattern of significantly reduced FA and λ_L that are similar to results in a mouse brain trauma model where FA and λ_L were both significantly reduced following trauma induction, the extent of which correlated with *in vitro* indices of axonal injury [74,75]. Although the results herein do not specifically demonstrate axonal disruption, alcohol is known to disrupt microtubules of cerebellar granule cell axons and Purkinje cell dendrites (3 months alcohol, sole source of fluid)[76] and axons in the extrapyramidal system, mesolimbic system, and several hypothalamic nuclei (16 months free-choice alcohol, alcohol-preferring rats)[77]. Thus, the effects of alcohol on DTI metrics in the genu could be interpreted as representing axonal injury.

The fimbria-fornix demonstrated reduced FA and elevated MD, λ_L, and λ_T during binge alcohol treatment. This pattern of changes is consistent with those observed in a transgenic rodent model: myelin-deficient jimpy mice have profound astrocytic hypertrophy and abnormally low FA and high MD, λ_L, and λ_T [78]. High alcohol exposure results in hypertrophied astrocytes in the hippocampus in mice (5 days alcohol, sole source of fluid) [79], and hippocampal astrogliosis, as quantified by immunohistochemical staining for vimentin in rats (4 days alcohol, intragastric) [80]. Thus the effects of alcohol on DTI metrics in the fimbria-fornix could be interpreted as representing astrocytic hypertrophy.

In conclusion, acute, quickly achieved, high doses of alcohol result in DTI-detectable effects on white matter that, although transient, corroborate findings in human alcoholics, demonstrating an anterior distribution of disrupted white matter fiber tracts with change toward normality with sobriety [12].

Acknowledgments

The research reported herein was supported by grants: A012388, AA017168, AA013521-INIA. The funders had no role in study design, data collection and analysis, decision to publish, or preparation of the manuscript.

The authors would like to recognize the contributions of Amy Collins, Matthew Serventi, Cheshire Hardcastle, Crystal Caldwell, Priya Asok, Juan Orduna, and Joey Montenegro for animal handling and MR data collection.

Author Contributions

Conceived and designed the experiments: AP EVS NMZ. Performed the experiments: NMZ. Analyzed the data: TR DM AP. Contributed reagents/materials/analysis tools: TR DM AP. Wrote the paper: EVS NMZ.

References

1. De la Monte SM (1988) Disproportionate atrophy of cerebral white matter in chronic alcoholics. Archives of Neurology 45: 990–992. PMID: 3415529
2. Harper C, Kril JJ (1985) Brain atrophy in chronic alcoholic patients: a quantitative pathological study. Journal of Neurology, Neurosurgery, and Psychiatry 48: 211–217. PMID: 3981189
3. Kril JJ, Butterworth RF (1997) Diencephalic and cerebellar pathology in alcoholic and nonalcoholic patients with end-stage liver disease. Hepatology 26: 837–841. PMID: 9328301
4. Harper CG, Kril JJ (1988) Corpus callosal thickness in alcoholics. Br J Addict 83: 577–580. PMID: 3382816
5. Tarnowska-Dziduszko E, Bertrand E, Szpak G (1995) Morphological changes in the corpus callosum in chronic alcoholism. Folia Neuropathologica 33: 25–29. PMID: 8673416
6. Pfefferbaum A, Sullivan EV, Hedehus M, Lim KO, Adalsteinsson E, Moseley M (2000) Age-related decline in brain white matter anisotropy measured with spatially corrected echo-planar diffusion tensor imaging. Magnetic Resonance in Medicine 44: 259–268. PMID: 10918325
7. Pfefferbaum A, Adalsteinsson E, Sullivan EV (2006) Dysmorphology and microstructural degradation of the corpus callosum: Interaction of age and alcoholism. Neurobiol Aging 27: 994–1009. PMID: 15964101
8. Pfefferbaum A, Rosenbloom MJ, Adalsteinsson E, Sullivan EV (2007) Diffusion tensor imaging with quantitative fiber tracking in HIV infection and alcoholism comorbidity: Synergistic white matter damage. Brain 130: 48–64. PMID: 16959813
9. Chanraud S, Zahr NM, Sullivan EV, Pfefferbaum A (2010) MR diffusion tensor imaging: A window into white matter integrity of the working brain. Neuropsychology Review 20: 209–225. doi: 10.1007/s11065-010-9129-7 PMID: 20422451
10. Sullivan EV, Pfefferbaum A (2013) Human Imaging Studies of Brain Circuitry Disrupted by Alcoholism. In: Noronha A, Cui C, Harris A, Crabbe JC, editors. Neurobiology of Alcohol Dependence. In Press ed.
11. Pfefferbaum A, Sullivan EV (2002) Microstructural but not macrostructural disruption of white matter in women with chronic alcoholism. Neuroimage 15: 708–718. PMID: 11848714
12. Pfefferbaum A, Rosenbloom M, Chu W, Sassoon SA, Rohlfing T, Pohl KM, et al. (2014) White matter microstructural recovery with abstinence and decline with relapse in alcoholism interacts with normal aging: A controlled longitudinal DTI study. The Lancet Psychiatry 202–212.
13. Mori S, van Zijl PC (2002) Fiber tracking: principles and strategies—a technical review. NMR Biomed 15: 468–480. PMID: 12489096
14. Jones DK (2010) Diffusion MRI: Theory, Methods, and Applications. Oxford: Oxford University Press.
15. Pierpaoli C, Barnett A, Pajevic S, Chen R, Penix L, Virta A, et al. (2001) Water diffusion changes in Wallerian degeneration and their dependence on white matter architecture. NeuroImage 13: 1174–1185. PMID: 11352623
16. Basser PJ, Jones DK (2002) Diffusion-tensor MRI: theory, experimental design and data analysis—a technical review. NMR Biomed 15: 456–467. PMID: 12489095
17. Pfefferbaum A, Sullivan EV (2003) Increased brain white matter diffusivity in normal adult aging: Relationship to anisotropy and partial voluming. Magnetic Resonance in Medicine 49: 953–961. PMID: 12704779
18. Pfefferbaum A, Sullivan EV (2005) Disruption of brain white matter microstructure by excessive intracellular and extracellular fluid in alcoholism: Evidence from diffusion tensor imaging. Neuropsychopharmacology 30: 423–432. PMID: 15562292
19. Song SK, Sun SW, Ramsbottom MJ, Chang C, Russell J, Cross AH (2002) Dysmyelination revealed through MRI as increased radial (but unchanged axial) diffusion of water. Neuroimage 17: 1429–1436. PMID: 12414282
20. Song SK, Yoshino J, Le TQ, Lin SJ, Sun SW, Cross AH, et al. (2005) Demyelination increases radial diffusivity in corpus callosum of mouse brain. Neuroimage 26: 132–140. PMID: 15862213

21. Choe AS, Stepniewska I, Colvin DC, Ding Z, Anderson AW (2012) Validation of diffusion tensor MRI in the central nervous system using light microscopy: quantitative comparison of fiber properties. NMR Biomed 25: 900–908. doi: 10.1002/nbm.1810 PMID: 22246940

22. Pfefferbaum A, Rosenbloom M, Rohlfing T, Sullivan EV (2009) Degradation of association and projection white matter systems in alcoholism detected with quantitative fiber tracking. Biol Psychiatry 65: 680–690. doi: 10.1016/j.biopsych.2008.10.039 PMID: 19103436

23. Pfefferbaum A, Sullivan EV, Carmelli D (2001) Genetic regulation of regional microstructure of the corpus callosum in late life. Neuroreport 12: 1677–1681. PMID: 11409738

24. Chanraud S, Reynaud M, Wessa M, Penttila J, Kostogianni N, Cachia A, et al. (2009) Diffusion tensor tractography in mesencephalic bundles: Relation to mental flexibility in detoxified alcohol-dependent subject. Neuropsychopharmacology 34: 1223–1232. doi: 10.1038/npp.2008.101 PMID: 18615012

25. Yeh PH, Simpson K, Durazzo TC, Gazdzinski S, Meyerhoff DJ (2009) Tract-Based Spatial Statistics (TBSS) of diffusion tensor imaging data in alcohol dependence: abnormalities of the motivational neurocircuitry. Psychiatry Research 173: 22–30. doi: 10.1016/j.pscychresns.2008.07.012 PMID: 19442492

26. Konrad A, Vucurevic G, Lorscheider M, Bernow N, Thummel M, Chai C, et al. (2012) Broad disruption of brain white matter microstructure and relationship with neuropsychological performance in male patients with severe alcohol dependence. Alcohol Alcohol 47: 118–126. doi: 10.1093/alcalc/agr157 PMID: 22214998

27. Sorg SF, Taylor MJ, Alhassoon OM, Gongvatana A, Theilmann RJ, Frank LR, et al. (2012) Frontal white matter integrity predictors of adult alcohol treatment outcome. Biol Psychiatry 71: 262–268. doi: 10.1016/j.biopsych.2011.09.022 PMID: 22047719

28. Li TK, Lumeng L, McBride WJ, Murphy JM (1987) Rodent lines selected for factors affecting alcohol consumption. Alcohol Alcohol Suppl 1: 91–96. PMID: 3426760

29. Grant KA, Bennett AJ (2003) Advances in nonhuman primate alcohol abuse and alcoholism research. Pharmacol Ther 100: 235–255. PMID: 14652112

30. Majchrowicz E (1975) Induction of physical dependence upon ethanol and the associated behavioral changes in rats. Psychopharmacologia 43: 245–254. PMID: 1237914

31. Faingold CL (2008) The Majchrowicz binge alcohol protocol: an intubation technique to study alcohol dependence in rats. Curr Protoc Neurosci Chapter 9: Unit 9 28. doi: 10.1002/9780471729259.mc09b01s10 PMID: 18729060

32. Dodero L, Damiano M, Galbusera A, Bifone A, Tsaftsaris SA, Scattoni ML, et al. (2013) Neuroimaging evidence of major morpho-anatomical and functional abnormalities in the BTBR T+TF/J mouse model of autism. PLoS One 8: e76655. doi: 10.1371/journal.pone.0076655 PMID: 24146902

33. Gozzi A, Agosta F, Massi M, Ciccocioppo R, Bifone A (2013) Reduced limbic metabolism and fronto-cortical volume in rats vulnerable to alcohol addiction. Neuroimage 69: 112–119. doi: 10.1016/j.neuroimage.2012.12.015 PMID: 23261637

34. Kong L, Lian G, Zheng W, Liu H, Zhang H, Chen R (2013) Effect of alcohol on diffuse axonal injury in rat brainstem: diffusion tensor imaging and aquaporin-4 expression study. Biomed Res Int 2013: 798261. doi: 10.1155/2013/798261 PMID: 24282821

35. Zahr NM, Mayer D, Rohlfing T, Orduna J, Luong R, Sullivan EV, et al. (2013) A mechanism of rapidly reversible cerebral ventricular enlargement independent of tissue atrophy. Neuropsychopharmacology 38: 1121–1129. doi: 10.1038/npp.2013.11 PMID: 23306181

36. USDHHS (2006) The Role of Biomarkers in the Treatment of Alcohol Use Disorders. In: Advisory SAT, editor.

37. O'Brien CP (2009) Alcoholism—The Dana Guide In: Foundation TD, editor: The Dana Foundation.

38. Majchrowicz E, Hunt WA (1976) Temporal relationship of the induction of tolerance and physical dependence after continuous intoxication with maximum tolerable doses of ethanol in rats. Psychopharmacology (Berl) 50: 107–112. PMID: 826949

39. Hunt WA, Redos JD, Dalton TK, Catravas GN (1977) Alterations in brain cyclic guanosine 3':5'-monophosphate levels after acute and chronic treatment with ethanol. J Pharmacol Exp Ther 201: 103–109. PMID: 15100

40. Adalsteinsson E, Hurd RE, Mayer D, Sailasuta N, Sullivan EV, Pfefferbaum A (2004) In vivo 2D J-resolved magnetic resonance spectroscopy of rat brain with a 3T clinical human scanner. Neuroimage 22: 381–386. PMID: 15110030

41. Pfefferbaum A, Adalsteinsson E, Sullivan EV (2004) In vivo structural imaging of the rat brain with a 3T clinical human scanner. Journal of Magnetic Resonance Imaging 20: 779–785. PMID: 15503335

42. Chronik B, Alejski A, Rutt BK (2000) Design and fabrication of a three-axis multilayer gradient coil for magnetic resonance microscopy of mice. Magma 10: 131–146. PMID: 10873203

43. Chronik BA, Alejski A, Rutt BK (2000) Design and fabrication of a three-axis edge ROU head and neck gradient coil. Magn Reson Med 44: 955–963. PMID: 11108634

44. Mayer D, Zahr NM, Adalsteinsson E, Rutt B, Sullivan EV, Pfefferbaum A (2007) In vivo fiber tracking in the rat brain on a clinical 3T MRI system using a high strength insert gradient coil. Neuroimage 35: 1077–1085. PMID: 17331742

45. Neeman M, Freyer JP, Sillerud LO (1991) A simple method for obtaining cross-term-free images for diffusion anisotropy studies in NMR microimaging. Magn Reson Med 21: 138–143. PMID: 1943671

46. Bodammer N, Kaufmann J, Kanowski M, Tempelmann C (2004) Eddy current correction in diffusion-weighted imaging using pairs of images acquired with opposite diffusion gradient polarity. Magn Reson Med 51: 188–193. PMID: 14705060

47. Jenkinson M (2003) A fast, automated, N-dimensional phase unwrapping algorithm. Magnetic Resonance in Medicine 49: 193–197. PMID: 12509838

48. Rohlfing T, Maurer CR (2003) Nonrigid image registration in shared-memory multiprocessor environments with application to brains, breasts, and bees. IEEE Transactions on Information Technology in Biomedicine 7: 16–25. PMID: 12670015

49. Rueckert D, Sonoda LI, Hayes C, Hill DL, Leach MO, Hawkes DJ (1999) Nonrigid registration using free-form deformations: application to breast MR images. IEEE Trans Med Imaging 18: 712–721. PMID: 10534053

50. Sullivan EV, Pfefferbaum A, Rohlfing T, Baker FC, Padilla ML, Colrain IM (2011) Developmental change in regional brain structure over 7 months in early adolescence: comparison of approaches for longitudinal atlas-based parcellation. Neuroimage 57: 214–224. doi: 10.1016/j.neuroimage.2011.04.003 PMID: 21511039

51. Mori S, Xue R, Crain B, Solaiyappan M, Chacko VP, van Zijl PCM (1999) 3D reconstruction of axonal fibers from diffusion tensor imaging using fiber assignment by continuous tracking (abs). Proceedings of the Seventh International Society for Magnetic Resonance in Medicine: 320.

52. Xu D, Mori S, Solaiyappan M, van Zijl PC, Davatzikos C (2002) A framework for callosal fiber distribution analysis. Neuroimage 17: 1131–1143. PMID: 12414255

53. Zhai G, Lin W, Wilber KP, Gerig G, Gilmore JH (2003) Comparisons of regional white matter diffusion in healthy neonates and adults performed with a 3.0-T head-only MR imaging unit. Radiology 229: 673–681. PMID: 14657305

54. Sullivan EV, Adalsteinsson E, Pfefferbaum A (2006) Selective age-related degradation of anterior callosal fiber bundles quantified in vivo with fiber tracking. Cerebral Cortex 16: 1030–1039. PMID: 16207932

55. Smith SM, Nichols TE (2009) Threshold-free cluster enhancement: addressing problems of smoothing, threshold dependence and localisation in cluster inference. Neuroimage 44: 83–98. doi: 10.1016/j.neuroimage.2008.03.061 PMID: 18501637

56. Alhassoon OM, Sorg SF, Taylor MJ, Stephan RA, Schweinsburg BC, Stricker NH, et al. (2012) Callosal white matter microstructural recovery in abstinent alcoholics: a longitudinal diffusion tensor imaging study. Alcohol Clin Exp Res 36: 1922–1931. doi: 10.1111/j.1530-0277.2012.01808.x PMID: 22551067

57. Smith SM, Jenkinson M, Johansen-Berg H, Rueckert D, Nichols TE, Mackay CE, et al. (2006) Tract-based spatial statistics: voxelwise analysis of multi-subject diffusion data. Neuroimage 31: 1487–1505. PMID: 16624579

58. Bell RL, Franklin KM, Hauser SL, Engleman EA (2013) Next Stop Dependence—Binge Drinking on the Road to Alcoholism: Preclinical Findings on its Neurobiology from Rat Animal Models In: Harris SB, editor. Binge Eating and Binge Drinking: Nova Science Publishers.

59. Martin-Fardon R, Weiss F (2013) Modeling relapse in animals. Curr Top Behav Neurosci 13: 403–432. doi: 10.1007/7854_2012_202 PMID: 22389178

60. Rodd ZA, Bell RL, Sable HJ, Murphy JM, McBride WJ (2004) Recent advances in animal models of alcohol craving and relapse. Pharmacol Biochem Behav 79: 439–450. PMID: 15582015

61. Oster SM, Toalston JE, Kuc KA, Pommer TJ, Murphy JM, Lumeng L, et al. (2006) Effects of multiple alcohol deprivations on operant ethanol self-administration by high-alcohol-drinking replicate rat lines. Alcohol 38: 155–164. PMID: 16905441

62. Rodd ZA, Bell RL, Kuc KA, Murphy JM, Lumeng L, McBride WJ (2009) Effects of concurrent access to multiple ethanol concentrations and repeated deprivations on alcohol intake of high-alcohol-drinking (HAD) rats. Addict Biol 14: 152–164. doi: 10.1111/j.1369-1600.2008.00140.x PMID: 19076927

63. Bell RL, Kimpel MW, Rodd ZA, Strother WN, Bai F, Peper CL, et al. (2006) Protein expression changes in the nucleus accumbens and amygdala of inbred alcohol-preferring rats given either continuous or scheduled access to ethanol. Alcohol 40: 3–17. PMID: 17157716

64. McBride WJ, Kimpel MW, Schultz JA, McClintick JN, Edenberg HJ, Bell RL (2010) Changes in gene expression in regions of the extended amygdala of alcohol-preferring rats after binge-like alcohol drinking. Alcohol 44: 171–183. doi: 10.1016/j.alcohol.2009.12.001 PMID: 20116196

65. Chen CM, Dufour MC, Yi HY (2004) Alcohol consumption among young adults ages 18–24 in the United States: Results from the 2001–2002 NESARC Survey. Alcohol Research and Health 28: 269–280.

66. Grant BF, Dawson DA, Stinson FS, Chou SP, Dufour MC, Pickering RP (2004) The 12-month prevalence and trends in DSM-IV alcohol abuse and dependence: United States, 1991–1992 and 2001–2002. Drug Alcohol Depend 74: 223–234. PMID: 15194200

67. Neighbors C, Larimer ME, Lostutter TW, Woods BA (2006) Harm reduction and individually focused alcohol prevention. Int J Drug Policy 17: 304–309. PMID: 17301880

68. Rutledge PC, Park A, Sher KJ (2008) 21st birthday drinking: extremely extreme. J Consult Clin Psychol 76: 511–516. doi: 10.1037/0022-006X.76.3.511 PMID: 18540744

69. Urso T, Gavaler JS, Van Thiel DH (1981) Blood ethanol levels in sober alcohol users seen in an emergency room. Life Sci 28: 1053–1056. PMID: 7219065

70. Touquet R, Csipke E, Holloway P, Brown A, Patel T, Seddon AJ, et al. (2008) Resuscitation room blood alcohol concentrations: one-year cohort study. Emerg Med J 25: 752–756. doi: 10.1136/emj.2008.062711 PMID: 18955613

71. Sagi Y, Tavor I, Hofstetter S, Tzur-Moryosef S, Blumenfeld-Katzir T, Assaf Y (2012) Learning in the fast lane: new insights into neuroplasticity. Neuron 73: 1195–1203. doi: 10.1016/j.neuron.2012.01.025 PMID: 22445346

72. Hofstetter S, Tavor I, Tzur Moryosef S, Assaf Y (2013) Short-term learning induces white matter plasticity in the fornix. J Neurosci 33: 12844–12850. doi: 10.1523/JNEUROSCI.4520-12.2013 PMID: 23904619

73. Toth A, Kovacs N, Perlaki G, Orsi G, Aradi M, Komaromy H, et al. (2013) Multi-modal magnetic resonance imaging in the acute and sub-acute phase of mild traumatic brain injury: can we see the difference? J Neurotrauma 30: 2–10. doi: 10.1089/neu.2012.2486 PMID: 22905918

74. Mac Donald CL, Dikranian K, Song SK, Bayly PV, Holtzman DM, Brody DL (2007) Detection of traumatic axonal injury with diffusion tensor imaging in a mouse model of traumatic brain injury. Exp Neurol 205: 116–131. PMID: 17368446

75. Mac Donald CL, Dikranian K, Bayly P, Holtzman D, Brody D (2007) Diffusion tensor imaging reliably detects experimental traumatic axonal injury and indicates approximate time of injury. J Neurosci 27: 11869–11876. PMID: 17978027

76. Paula-Barbosa MM, Tavares MA (1985) Long term alcohol consumption induces microtubular changes in the adult rat cerebellar cortex. Brain Research 339: 195–199. PMID: 4040788

77. Putzke J, De Beun R, Schreiber R, De Vry J, Tolle T, Zieglgansberger W, et al. (1998) Long-term alcohol self-administration and alcohol withdrawal differentially modulate microtubule-associated protein 2 (MAP2) gene expression in the rat brain. Brain Res Mol Brain Res 62: 196–205. PMID: 9813323

78. Harsan LA, Poulet P, Guignard B, Parizel N, Skoff RP, Ghandour MS (2007) Astrocytic hypertrophy in dysmyelination influences the diffusion anisotropy of white matter. J Neurosci Res 85: 935–944. PMID: 17278151

79. Satriotomo I, Miki T, Itoh M, Ameno K, Ijiri I, Takeuchi Y (2000) Short-term ethanol exposure alters calbindin D28k and glial fibrillary acidic protein immunoreactivity in hippocampus of mice. Brain Res 879: 55–64. PMID: 11011006

80. Kelso ML, Liput DJ, Eaves DW, Nixon K (2011) Upregulated vimentin suggests new areas of neurodegeneration in a model of an alcohol use disorder. Neuroscience 197: 381–393. doi: 10.1016/j.neuroscience.2011.09.019 PMID: 21958862